



Fog Detection
Algorithm Theoretical Basis Document

Code: NMSC/SCI/ATBD/FOG
Issue: 1.0 Date:2012.12.21
File: NMSC-SCI-ATBD-FOG_v1.0.hwp
Page: 18



Fog Detection(FOG) Algorithm Theoretical Basis Document (FOG-v1.0)

NMSC/SCI/ATBD/FOG, Issue 1, rev.0
2012.12.12



Fog Detection
Algorithm Theoretical Basis Document

Code: NMSC/SCI/ATBD/FOG
Issue: 1.0 Date:2012.12.21
File: NMSC-SCI-ATBD-FOG_v1.0.hwp
Page: 18

REPORT SIGNATURE TABLE

Function	Name	Signature	Date
Prepared by	Lee, Jung Rim		2013. 3. 4
Reviewed by			
Authorised by			



Fog Detection
Algorithm Theoretical Basis Document

Code: NMSC/SCI/ATBD/FOG
Issue: 1.0 Date:2012.12.21
File: NMSC-SCI-ATBD-FOG_v1.0.hwp
Page: 18

DOCUMENT CHANGE RECORD

Version	Date	Pages	Changes

Table of Contents

1. Overview
2. Background and purpose
3. Algorithm
 - 3.1 Theoretical Background
 - 3.2 Methodology
 - 3.3 Calculation Process
 - 3.4 Evaluation
 - 3.4.1 Evaluation Method
 - 3.4.2 Evaluation Material
 - 3.4.3 Time Space Concurrence Method
 - 3.4.4 Evaluation Result Analysis
4. Interpretation Method of Calculation Result
5. Problems and Area of Improvement
6. References

List of Tables

Table 1 : Input data for the FOG2 Algorithm.

Table 2 : Criteria used in the FOG2 algorithm.

Table 3 : INDEX values for FOG2 result.

Table 4 : QC parameters using bit method.

Table 5 : Description of the auxiliary data for FOG2 validation.

Table 6 : The collocation methods for FOG2 validation.

List of Figures

- Figure 1 : RTM simulation results. The value of $3.7\mu\text{m}$ - $10.8\mu\text{m}$ changes as a function of solar zenith angle and effective radius(Re) in each graph. Different colors varied from light blue to dark blue in the graph represent different Re (2, 4, 8, 16, 32, 64), and each graph (a~f) is the simulation results for different cloud optical depth(COT) values (2, 4, 8, 16, 32, 64).
- Figure 2 : The flowchart of FOG2 algorithm
- Figure 3 : SWIR-IR1 images on fog case (near red box) at 1833 UTC (a) and 2133 UTC (b) on January 8th and 0033 UTC (c) and 0333 UTC (d) on January 9th in 2008.
- Figure 4 : Plots of SWIR-IR1 (K) according to the solar zenith angle (degree) in the red box of figure 3.
- Figure 5 : FOG2 validation methods.
- Figure 6 : The validation results from 1 to 4 in October 2008. (a) and (b) represent GTS for East-Asia and Ground observation data for Korea respectively.
- Figure 7 : The validation results from 1 through 4 in October 2008. (a) and (b) represent the validation results with GTS over East-Asia and with ground observation data over Korean peninsula, respectively.
- Figure 8 : MTSAT-1R SWIR at 02 UTC 7 Nov. 2007 (a) and fog detection results on IR1 image (b~f)



List of Acronyms

COMS	Communication, Ocean, and Meteorological Satellite
CMDPS	Coms Meteorological Data Processing System
CSI	Critical Success Index
FAR	False Alarm Rate
GOES	Geostationary Operational Environmental Satellites
IR	Infrared image
MTSAT-1R	Multi-functional Transport SATellite
PC	Proportion Correct
POD	Probability of Detection
POFD	Probability of False Detection
RTM	Radiative Transfer Model
SWIR	ShortWave Infrared
VIS	Visible image
WV	WaterVapor image

1. Overview

Poor visibility due to fog can cause serious accident not only on the ground but also air and sea transportation, leading significant damage on human life and their property. Accurate detection of fog area and forecasting the duration time are the important measures to prevent these accidents and to reduce loss.

This paper is the algorithm theoretical basis document of CMDPS fog detection algorithm. Physical background, general methodology and the purpose of the estimation are described in Chapter 2, and in Chapter 3, theoretical background, derivation methodology and the estimation processes are described. Finally, currently existing problems and possibilities for improvement are described in detail.

2. Background and Purpose

Fog is directly observed by visual measurement at the ground weather station, showing the fog information around the station of observation. Therefore, it is hard to obtain information on fog at a place without a observatory station, and it is even harder to make accurate observation at night. However, as satellite enables observation throughout wider area with shorter interval, it is an important measure to obtain information on fog area settled throughout wide area.

Fog forecast using satellite data is calculated utilizing the feature that the fog emission rate on short wave infrared channel is lower than that on infrared channel (Eyre et al., 1984; Turner et al., 1986; Dybbroe et al., 1993; Bendix, 2002). While fog emission on infrared channel is close to 1, that on short wave infrared channel is as low as 0.7~0.8 (Ellord 1995; Wetzal et al. 1996; Lee et al. 1997). Thus, Fog/low level cloud can be detected at night by using temperature difference between two channels. However, during day time, as short wave infrared channel observes not only substance emitted from the ground surface but also reflecting substance, the luminance temperature difference has different characteristics at day and night, causing discontinuity of fog detection between day and night. On visible channel, fog has higher reflectivity, so thick fog area can be distinguished during the day, and fog and high level cloud can be more or less distinguishable by brightness temperature of infrared channel. (Gultepe et al., 2007).

Even though fog occurs when it touches the ground, its property of low level cloud

makes fog detection using satellite very difficult (Bendix et al., 2005). Fog has different optical characteristics depending on topology (ocean, ground), and particularly in an area with complicated geological features like Korean peninsular, locally occurring fog is difficult to detect due to the limit of space resolution of satellites. In addition, as short wave infrared channel, which is the most important measure of fog detection, has different observation characteristics between day and night, discontinuity of fog detection is caused between day and night.

In this study, we developed an algorithm that uses adaptive threshold to minimize the discontinuity of fog detection among day/night and seasons. To remove pollutant pixel from the ground that largely take place at twilight, reflectivity on clear sky visible channel was used, and to remove pollution by cloud pixel, channel difference method (IR1-IR2, IR1-WV) and infrared channel brightness temperature were used to minimize pollutant pixel. We tried to calculate the final fog area by applying the fog characteristics of time continuity and space homogeneity to the algorithm.

3. Algorithm

3.1. Theoretical Background

In this algorithm, dual channel difference between SWIR and IR1($DCD_{SWIR-IR1}$) is mainly used to detect fog area with the characteristic having different emission over fog. This characteristic is shown as short wave infrared channel measures not only emission from the ground but also the reflectivity during the day. In particular, for the water droplet with small particle as fog, $DCD_{SWIR-IR1}$ differs greatly depending on solar zenith angle(Lee et al. 1997; Turk et al. 1998; Schreiner et al., 2007). Change of $DCD_{SWIR-IR1}$ following the solar zenith angle is shown in Fig. 1, as a result of simulative radiation changing the effective radius (Re) that indicates the size of the water droplet. In the chart, the color of lines varies from light blue to dark navy due to the variation of Re (from 2 to 4, 6, 16, 32, and 64), and each graph (a, b, c, d, e, and f) shows the different result according to the cloud optical depth(COT) (from 2 to 4, 8, 16, 32, and 64). In all figures, $DCD_{SWIR-IR1}$ has negative value during the night (solar zenith angle $> 90^\circ$), but as the sun rises(solar zenith angle $< 90^\circ$), $DCD_{SWIR-IR1}$ changes to the positive values. When the effective radius is large (dark navy), the change is not too significant, but when the effective radius is small (light blue), the difference between the channels changes

greatly. The difference increases when solar zenith angle is between $60^\circ \sim 90^\circ$ according to the solar zenith angle, and it has relatively constant value when the angle is smaller than 60° . This trend is shown even when COT changes. When COT increases, the variable breadth (lower value at night, higher value during the day) of small droplet (small Re) increases. Therefore, in this algorithm, adaptive threshold was applied to $DCD_{SWIR-IR1}$ that changes according to the solar zenith angle, using the optical property of fog having small droplet particle.

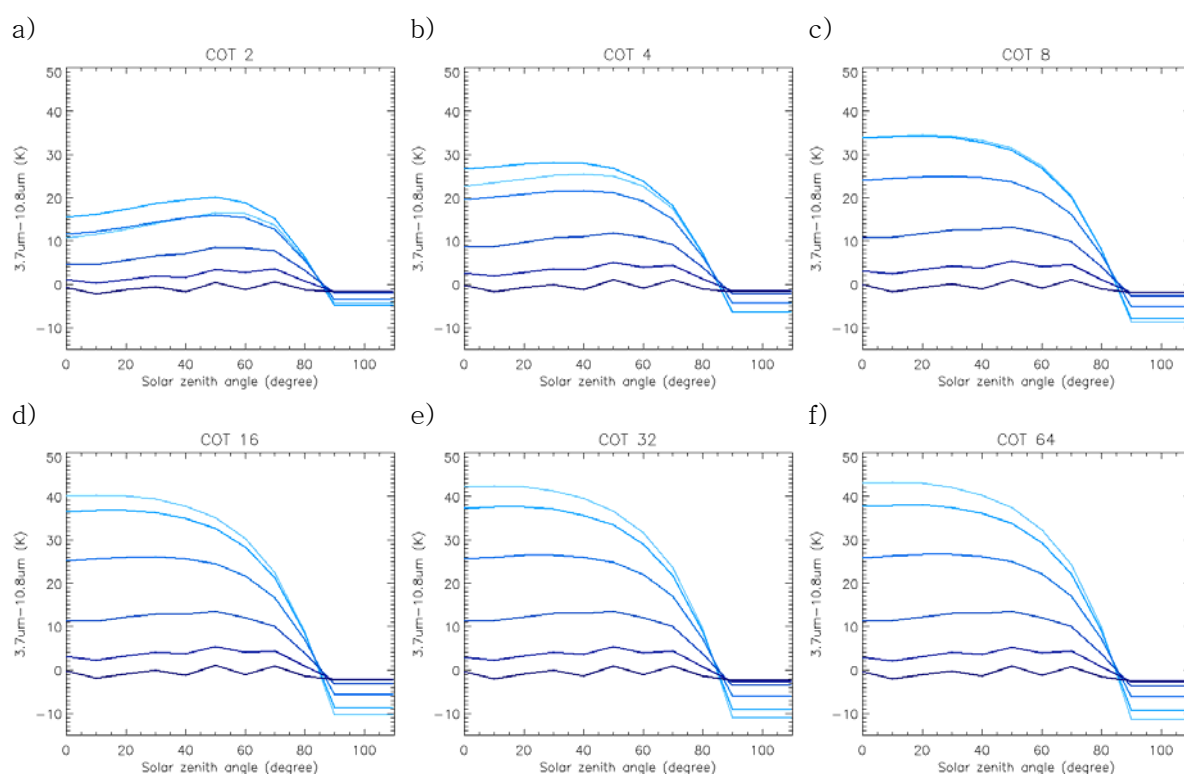


Figure 1. RTM simulation results. The value of $3.7\mu\text{m}-10.8\mu\text{m}$ changes as a function of solar zenith angle and effective radius(Re) in each graph. Different colors varied from light blue to dark blue in the graph represent different Re (2, 4, 8, 16, 32, 64), and each graph (a~f) is the simulation results for different cloud optical depth(COT) values (2, 4, 8, 16, 32, 64).

3.2. Methodology

In this algorithm, fog area is detected by applying adaptive threshold to $DCD_{SWIR-IR1}$ that changes greatly according to solar zenith angle, to make continuous fog detection

for day/night and each season. Based on Fig. 1, day time (solar zenith angle <60), twilight ($90 < \text{solar zenith angle} < 60$), and night (solar zenith angle >90) were divided according to solar zenith angle. Constant negative value and positive value are used as the threshold for night and day time, respectively, and adaptive threshold changing according to solar zenith angle was used for twilight. To remove cloud contaminated pixel and the noise from the ground, the difference between two infrared channels and clear sky reflectance of visible channel were used. Also, the properties of fog which stays long retaining the shape, and spatially homogeneous were used for this algorithm.

3.3. Calculation Process

Flow chart of fog detection algorithm is shown in Fig. 2. This algorithm estimates final fog coverage and QC flag through the whole process including reading data input, threshold test, time continuity check, and some threshold test using visible and other infrared channels.

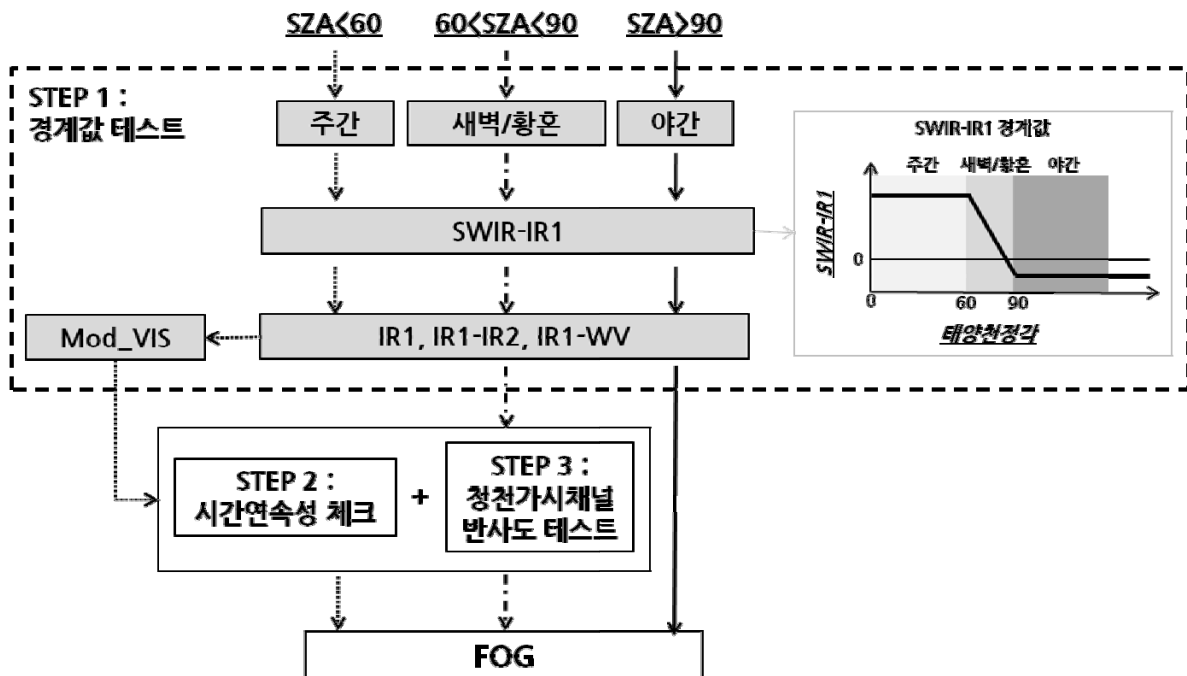


Figure 2. The flowchart of FOG2 algorithm

Input data

To detect fog, basically short wave infrared channel and infrared channel 1 data were

used as input data to calculate the dual channel difference. Visible channel reflectivity is also used as a measure to detect fog during day time. Data from all 5 channels of COMS satellite are used to eliminate contaminated pixel by cloud and the surface. For auxiliary data, 15 days minimum reflectivity composite field is utilized to remove contamination from the surface at twilight and day time. Previously calculated fog detection results were also introduced to check temporal consistence of fog area. Solar zenith angle to distinguish day/night is used as input data, and land/sea mask is used to calculate quality information (Table 1). Fog is calculated for satellite zenith angle of 65° and under, same as other CMDPS outputs.

Table 1. Input data for the FOG2 Algorithm.

	Data	Grid size (space resolution)
COMS	VIS	2750 × 2750 (4km)
	SWIR	2750 × 2750(4km)
	WV	2750 × 2750(4km)
	IR1	2750 × 2750(4km)
	IR2	2750 × 2750(4km)
Composite Input	CS_Refl	2750 × 2750(4km)
Static Input	Land/sea mask	2750 × 2750(4km)
Dynamic Input	Solar zenith angle	2750 × 2750(4km)
	Satellite zenith angle	2750 × 2750(4km)

STEP 1 : Threshold test

Fog detection algorithm mainly consists of threshold tests including $DCD_{SWIR-IR1}$, visible channel reflectivity and the dual channel differences between IR channels. Threshold values used in the algorithm are shown in Table 2. Fog detection algorithm changes depending on the time (night, twilight and day time). Each algorithm uses different threshold test, respectively. For nights, threshold checks on SWIR-IR1, IR1-IR2, IR1-WV, and IR1 are carried on for fog classification. In addition, visible reflectance difference between current and previous 15 days minimum value is tested during daytime, and the threshold values vary with solar zenith angle. One more simple threshold test on corrected visible channel reflectivity (adjusted by solar zenith angle) is

added. Detailed explanation of each test is given in STEP1.1~STEP1.4.

Table 2. Criteria used in the FOG2 algorithm.

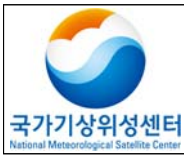
Criteria	Night	Dawn/dusk	Day time	Explanation
Solar zenith angle	89° and up	60°~ 89°	Under 60°	Day/night distinguished
SWIR-IR1	-9.5~-2.5	Adaptive threshold	15~50	Low level cloud separated
IR1-IR2	Adaptive threshold is used			High level cloud removed
IR1-WV	Adaptive threshold is used			High level cloud removed
IR1	260 K and up	260 K and up	260 K and up	High level cloud removed
vis_alb-CS_refl	-	Adaptive threshold~40	Adaptive threshold~40	Ground surface effect removed
mod_sza_alb	-	-	25~55	Fog area

STEP 1.1 : Day/night distinction

As characteristics of shortwave infrared measurement which is mainly used in fog detection algorithm differs depending on day or night, and visible channel can be used for day time fog detection, different algorithms are used for day time, twilight, and night. Day time, twilight, and night are classified according to solar zenith angle. When solar zenith angle is larger than 89°, it is night, if the angle is between 60°~89° , it is twilight, and if the angle is smaller than 60°, it is day time.

STEP 1.2 : SWIR-IR1

As short wave infrared channel, which is mainly used in fog detection, has different observatory features day and night (at night, only emission is measured, while during the day, both reflectance and emission is measured together), different thresholds are used for day, twilight, and night. The variation of the difference between SWIR and IR1 in fog area over time is shown in Fig. 3. The fog in this example developed widely throughout eastern region and the coast of China from January 8 to 9, 2008. a), b), c), and d) indicate the observation time of 1833 UTC, 2133 UTC on 8th, 0033 UTC, and 0333 UTC on 9th, respectively. Dark color in the image indicates smaller value, and light color indicates larger value in DCD, and the area with boxes represent fog. Compared to images of a) and b), the fog area in the images of c) and d) shows lighter color than



Fog Detection

Algorithm Theoretical Basis Document

Code: NMSC/SCI/ATBD/FOG
Issue: 1.0 Date:2012.12.21
File: NMSC-SCI-ATBD-FOG_v1.0.hwp
Page: 18

the background; because SWIR channel measures reflective substance also during the day. Fog area (around the red box) shows smaller value (darker color) than surroundings in the night time image and larger value (lighter color) during the day, showing that it has different property between day and night. Fig. 4 shows the plotted values of the pixels in the red box, and we can see the variation of the values according to solar zenith angle. The graph shows negative value when solar zenith angle is larger than 90, and as solar zenith angle becomes smaller under 90 degrees, the values in the box rapidly increases up to 30 K when solar zenith angle is about 60 degree.

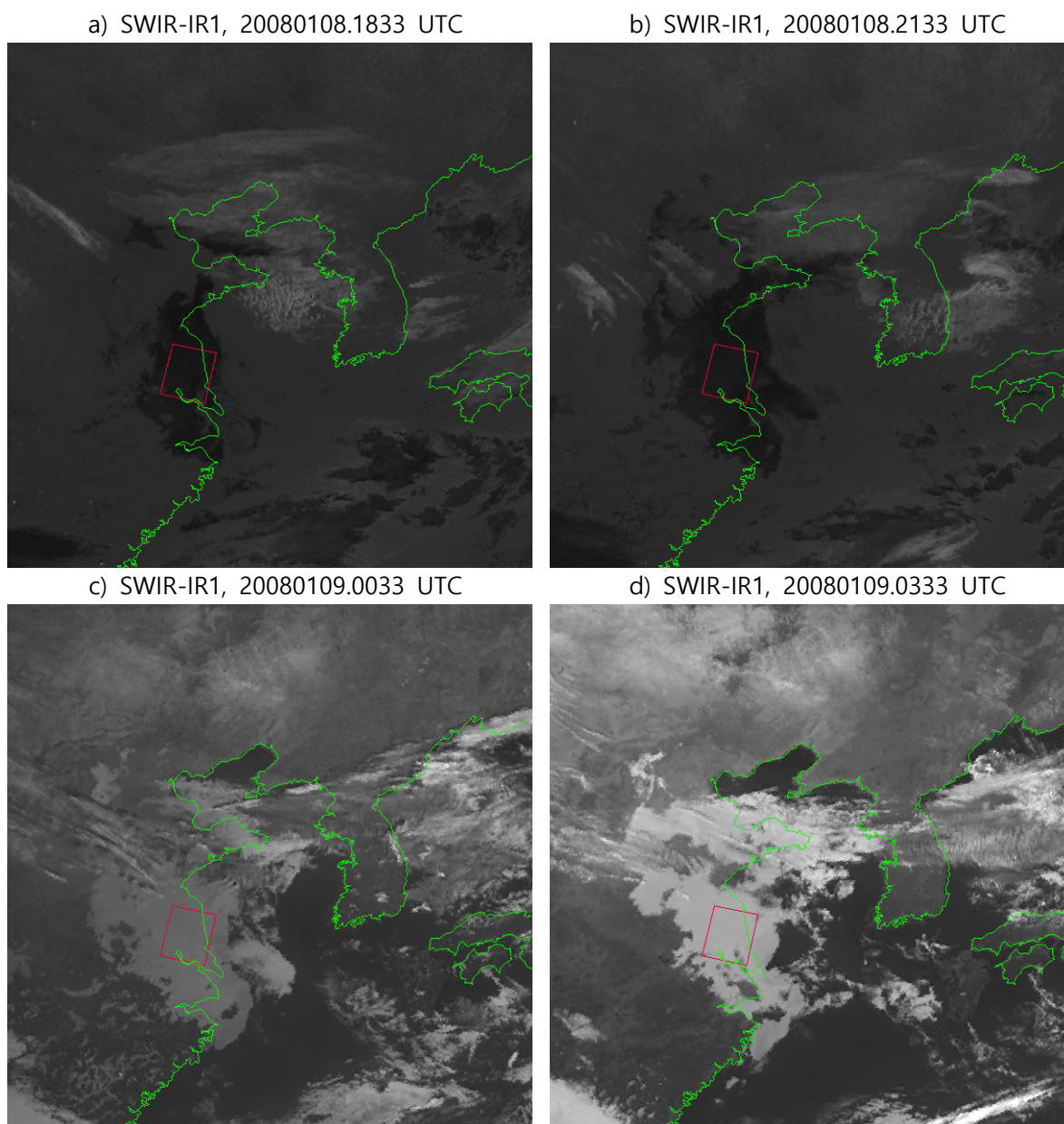


Figure 3. SWIR-IR1 images on fog case (near red box) at 1833 UTC (a) and 2133 UTC (b) on January 8th and 0033 UTC (c) and 0333 UTC (d) on January 9th in 2008.

This result matches with the simulative radiation in Fig. 1. Therefore, in this algorithm, we set up dynamic threshold according to solar zenith angle. The threshold range of $-9.5 \sim -2.5$ (K) is used for night when solar zenith angle is larger than 90, and $15 \sim 26$ (K) is used for day time when solar zenith angle is smaller than 60. In twilight when solar zenith angle is $60 \sim 90$, SWIR-IR1 varies, and dynamic threshold is calculated as follows:

$$\text{swir_ir1_thr_min} = 72.0048 - 0.828323 \cdot \theta_{\text{degree}} - 7$$

$$\text{swir_ir1_thr_max} = 72.0048 - 1.5 \cdot \theta_{\text{degree}} + 60.5$$

Here, θ_{degree} is solar zenith angle, and it this algorithm detects fog when the value of SWIR-IR1 is between swir_ir1_thr_min and swir_ir1_thr_max .

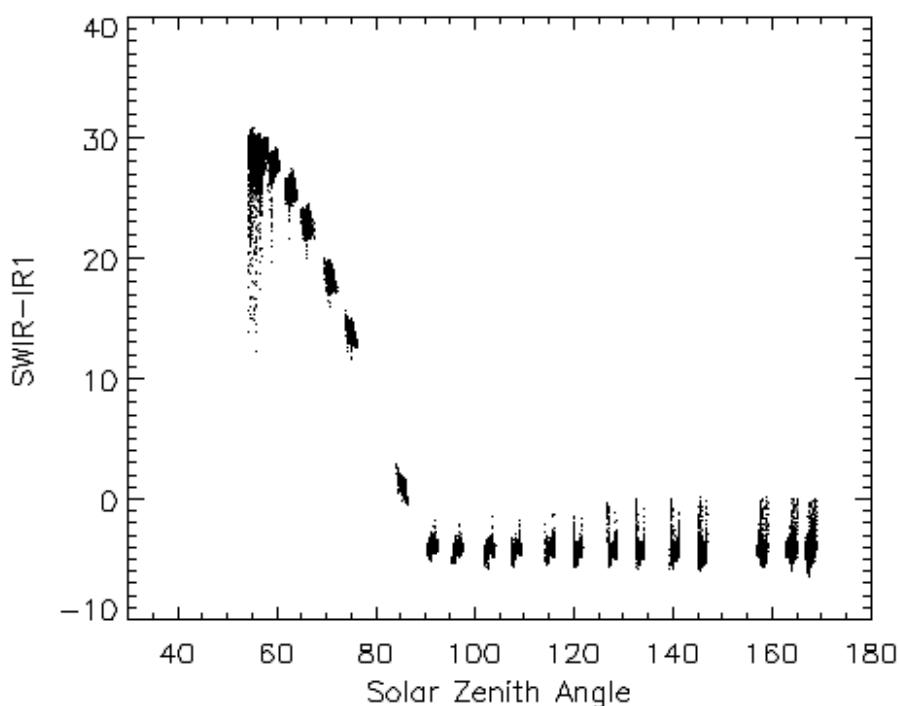


Figure 4. Plots of SWIR-IR1 (K) according to the solar zenith angle (degree) in the red box of fig. 3.

STEP 1.3 : IR1-IR2, IR1-WV, IR1

To remove high level cloud such as cirrus and to remove pollutant pixel by ground surface, threshold was established for infrared 1 luminance temperature and infrared channel difference. Fig. 5 shows the example where pollutant pixel by cloud is removed through adjustment. (a) is the fog detection result on January 8, 2008, and (b) is the detection result after adjustment using IR1-IR2. It is shown that the pollutant pixel which had taken place in Japan and surrounding sea is largely removed. (c) is the fog detection result of 0233 UTC on November 7, 2007, and (d) is the detection result after adjustment using IR1-WV. After adjustment, pollutant pixel from ground surface in Chinese continent and cloud pollutant in North Pacific were largely removed. The threshold of each channel difference method has adaptive threshold differing according

to infrared channel luminance temperature (K). Each threshold is like follows:

IR1-IR2 infrared difference threshold : Fog is detected when the value is between
 $thr_min_dtb45 < IR1-IR2 < thr_max_dtb45$

$$thr_min_dtb45 = -37.4793 + IR1 \cdot 0.132949 - 1$$

$$thr_max_dtb45 = -37.4793 + IR1 \cdot 0.132949 + 1$$

IR1-WV infrared difference threshold :Fog is detected when IR1-WV is higher than
 thr_dtb43

$$thr_dtb43 = 299 - IR1$$

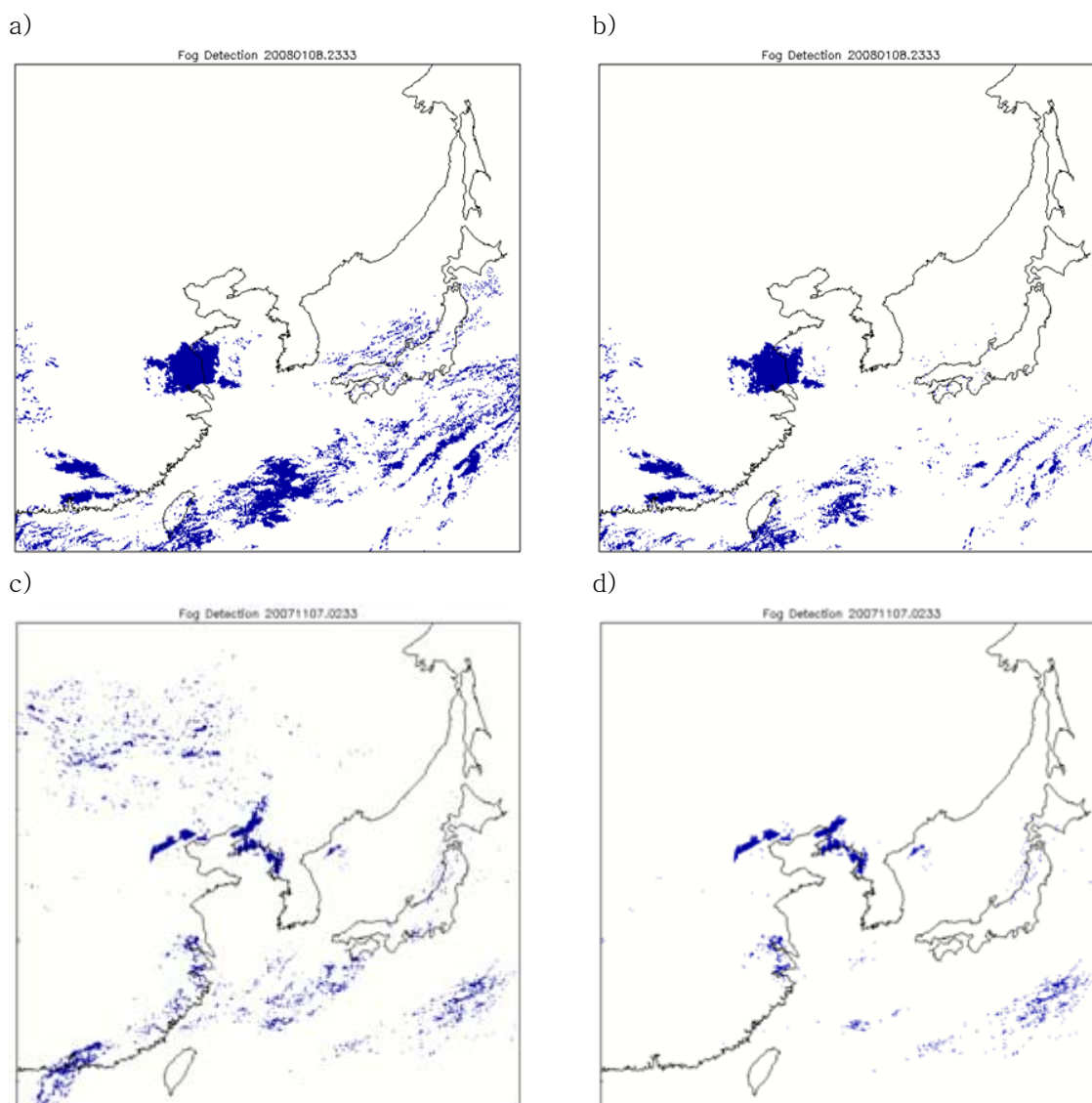


Figure 5. Example images on IR corrections. (b) image is the results of IR1-IR2 correction on (a), and (d) image is the results of IR1-WV correction on (c).

STEP 1.4 : mod_sza_alb

Fog has high reflectivity in visible channel. Thus, fog area is easily detected in visible image using the properties such as high reflectivity, space homogeneity and temporal consistency of fog. In this algorithm, visible channel reflectivity is used in day time fog detection. As the reflectivity of visible channel changes according to factors like the position of the sun, adjustment is made in advance using solar zenith angle.

$$mod_sza_alb = ch1_alb / \cos(\theta_{rad}) \quad (1)$$

Here, $ch1_alb$ and mod_sza_alb are reflectivity of visible channel and modified reflectivity using solar zenith angle(θ_{rad}), respectively. The visible channel reflectivity after modification becomes larger overall, and the change is barely shown following the daily variation of solar zenith angle (Refer to Step 2: Solar zenith angle adjustment in 3.3 Calculation Process of Sea ice/Snowdrift ATBD). In this algorithm, the threshold range of the modified visible reflectivity was 25-55 K.

STEP 2 : Correction with clear sky visible channel reflectivity adjustment

When fog area is detected through these threshold testes, the properties of fog are changed over time because the position of the sun and the characteristics of satellite image are changed. In particular, from night to dawn, large amount of contaminated pixel from the surface is shown. To remove those pixels, minimum visible reflectivity for previous 15 days is used as a clear background condition, and is applied like follows:

$$drefl = ch1_alb - csr_refl$$

Here, csr_refl is the minimum visible reflectivity for previous 15 days, and $ch1_alb$ is visible reflectance. Fog are is detected when calculaed $drefl$ is between thr_min_drefl and thr_max_drefl .

$$thr_min_drefl = 3 \cdot \cos(\theta_{rad}) + 4 - \exp(\theta_{degree}/10.) / 10000$$

$$thr_max_drefl = 40$$

STEP 3 : Time continuity test

When adjustment is made using clear sky reflectivity in STEP 2, sometimes fog area is removed at dawn due to the characteristics of SWIR. To recover those area, temporal consistency, which is one of the main property of fog is introduced using the fog detection result of immediate previous image. In this method, pixels that have been decided as fog in the previous image is classified again as fog when the pixel is passed by the other threshold test. Consequently, fog pixel which had been removed in STEP 2 is recovered as fog pixel. This method is only applied to twilight and day time when clear sky visible reflectivity test is applied.

Fog detection result

Fog detection result of FOG2 has value between 0 and 4 as shown in Table 3. 0 indicates clear sky and 1~4 indicate fog pixel. "datw_asmp" and "day_asmp" expressed as 1 is the pixel that passed the time continuity test in STEP 3, adding reliability to fog detection result.

Table 3. INDEX values for FOG2 result.

Parameter	Index
night fog	2
datw	3
datw_asmp	1
day	4
day_asmp	1
no	0
unavail	-999

Quality information

Quality information of FOG2 is produced for total 5 items of sea/land, day/night, use of CS_Refl and previous fog detection result, and result of CMDPS cloud detection. Details are shown in Table 4.

Table 4. QC parameters using bit method.

Condition	QC bit
land/coast	128
twilight	+96
day	+64
night	+32
csr_ir(ix,jy) /= real_unavail	+16
fog_prev(ix,jy)/=indx_fog_no .OR. fog_prev(ix,jy)/=int_unavail	+8
cld(ix,jy)%prob == 5	+5
cld(ix,jy)%prob == 4	+4
cld(ix,jy)%prob == 3	+3
cld(ix,jy)%prob == 2	+2
cld(ix,jy)%prob == 1	+1

3.4. Validation

3.4.1. Validation method

Observation data from the ground station are used for verification, thus, pixels around the ground observation data are only validated. For validation, 5 statistical methods are used including Probability of detection (POD), which indicates the ratio of fog pixel detection same as the result of auxiliary evaluation data and Probability of false detection (POFD), that shows the ratio of false detection as fog pixel compared to auxiliary evaluation data (Fig. 6). It means good match when the value is close to 1 in the case of POD, PC, and CSI, and when the value is close to 0 in the case of POFD and FAR.

검증보조자료

		Yes	No
산출값	Yes	A	B
	No	C	D

POD(probability of detection) : $A/(A+C)$

POFD(probability of false detection) : $B/(B+D)$

FAR(false alarm ratio) : $B/(A+B)$

PC(proportion correct, accuracy) : $(A+D)/N$

CSI(critical success index, threat score)

: $A/(A+B+C)$

Figure 6. FOG2 validation methods.

3.4.2. Evaluation Data

Auxiliary data for validation is shown in Table 5. Fog is evaluated with weather phenomena factor from the ground observation data. It is defined as ground fog when current weather is 40~49 and it is defined as clear sky in other cases.

Table 5. Description of the auxiliary data for FOG2 validation.

Auxiliary data	Area	Time resolution	Number of observation points
GROUND	Korean peninsular	1 hour	89
GTS	Global (Only Eastern Asian region was evaluated)	3 hours (00, 03, 06, 09, 12, 15, 18, 21 UTC)	3523

3.4.3. Method of Time and Space Concurrence

Auxiliary fog evaluation data, GROUND and GTS data are observed every 1 hour.

However, in the case of GTS, it is evaluated every 3 hours because regular data is received every 3 hours for Eastern Asian region, which is the fog evaluation area. Therefore, GROUND data is evaluated with the fog detection result within 30 minutes around every hour and GTS data is evaluated with fog detection result within 30 minutes around every 3 hours. In terms of space, as GROUND and GTS data are both point observation data, it is compared with fog detection result of 3 X 3 pixel around the observation location. Here, it is defined as CMDPS fog pixel when at least 5 pixels out of 3X3 pixels are detected as fog.(Table 6).

Table 6. The collocation methods for FOG2 validation.

Auxiliary data	Temporal resolution	Spatial resolution	Collocation of fog detected result		
			Time	Space	Base data
GROUND	1 hour	Point of observation	Within \pm 30 minutes	3 \times 3	GROUND
GTS	3 hours	Point of observation	Within \pm 30 minutes	3 \times 3	GTS

3.4.4. Evaluation Result Analysis

As fog is evaluated with the eye observation data on the ground, it is quite different from the observation from satellite. In particular, while ground observation observes fog regardless the presence of high level cloud, satellite cannot detect fog when there is high level cloud, unable to obtain information on ground surface. Due to those differences, the validation result contains a lot of error besides the performance of fog detection algorithm. Fig. 7 is the evaluation of the result of hourly fog detection on October 1st to 4th, 2008. (a) is the evaluation result of GTS in Eastern Asia, and (b) is evaluation result in Korea. Red and blue bar in the graphs show the result of POD and CSI, respectively, and green line indicates the number of points on which fog is observed on the ground. Both POD and CSI show better evaluation result when the value is closer to 1. Both evaluations show a trend to be proportionate to the number of fog observation point on the ground. It shows that the evaluation value are low when there is fewer fog on the ground, and it is not significant to make statistical monitoring of fog which occurs occasionally. In this case, local fog occurred due to complex topology in Korean peninsular. When any navigation error takes place in the satellite, fog detection area can moves and evaluation quality may be reduced.

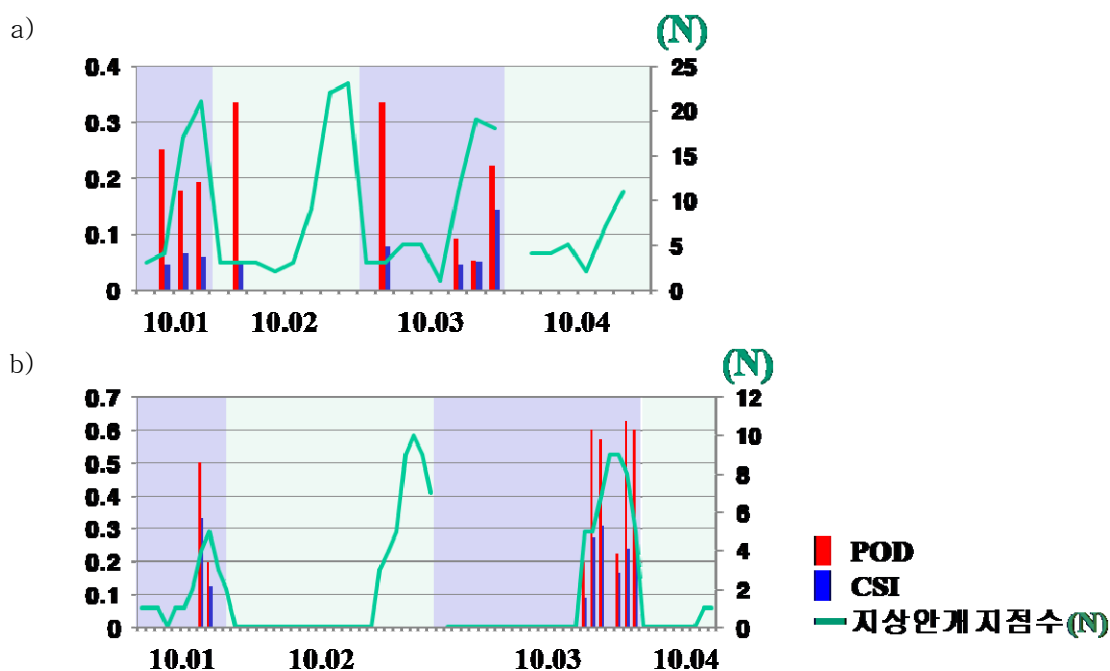
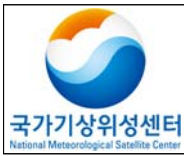


Figure 7. The validation results from 1 through 4 in October 2008. (a) and (b) represent the validation results with GTS over East-Asia and with ground observation data over Korean peninsula, respectively.

4. Analysis Method of Calculation Result

Detection result of fog occurred on November 6 and 7, 2007 in Manchuria, China was analyzed (Fig. 8). (a) shows SWIR image of UTC on November 7, 2007. In SWIR image, fog/low level cloud area look dark as the sun rises. In this image, dark and thick fog are shown as black area around Beijing, Manchuria, and South Eastern China. (b)-(f) show the fog detection result of the case over infrared channel image. The light blue pixel in the image is from "threshold test" at night or "threshold test +clear sky visible reflectivity test" in day/twilight. Orange pixel is the fog detected through "threshold test + time continuity test" in day/twilight and this is a relatively reliable result with less possibility of pollutant pixel suddenly appearing from cloud or ground surface. Magenta color boxed in the image indicates points on which fog is reported on the ground (GTS). The detection results b (6th, 1733) through f (7th,0533) show the continuous process of formation, development and disappearance of fog. This also conforms well with the fog point on the ground (GTS). While fog was reported in Manchuria as (d), (e), and (f), there are some points that were not detected as fog in the fog detection



Fog Detection
Algorithm Theoretical Basis Document

Code: NMSC/SCI/ATBD/FOG
Issue: 1.0 Date:2012.12.21
File: NMSC-SCI-ATBD-FOG_v1.0.hwp
Page: 18

result. This is because fog was not detected as there was high level cloud as seen in infrared image. In 2333 UTC (d), fog reported from Northern China to Russia was not detected on some locations. These are the pixels that are not detected as fog because of the thin high level cloud and cold ground surface temperature in high latitude area. The pollutant pixels in Northern China shown in 0233 UTC (e) and 0533 UTC (f) during day time are caused by ground surface and the pixels on the edge of the long cloud band stretched on the Southern sea of Japan are also the pollutant pixels by cloud.

In addition, the result of CMPDS fog detection expressed in National Meteorological Satellite Center is marked as "Possible fog area" and "Fog area". "Possible fog area" is #1 of CMDPS FOG result and this means that the area is not detected as fog at current moment, but has been detected as fog in the previous image. Day time fog from # 2 to 4 and fog at twilight and night are marked as "Fog area".

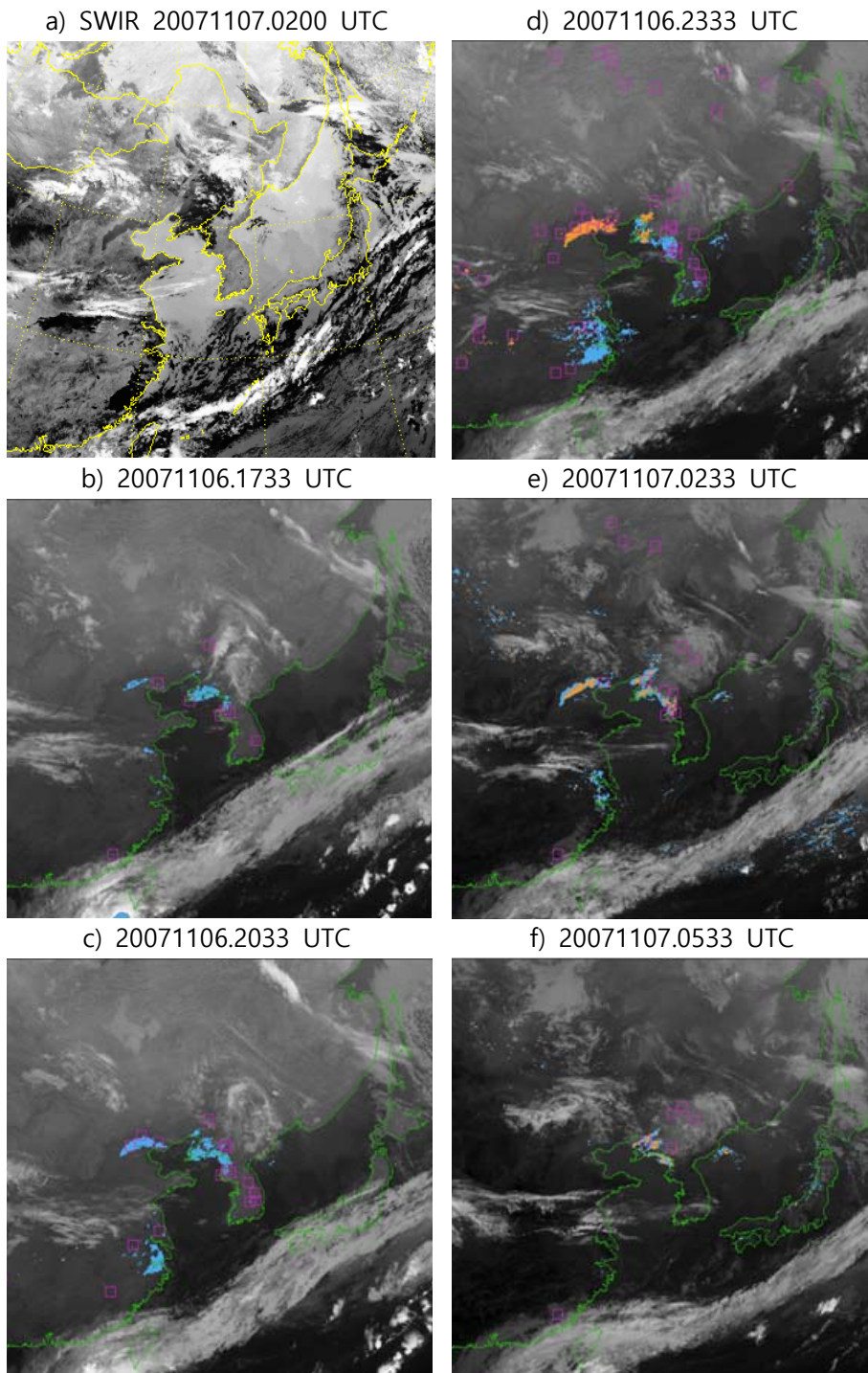


Figure 8. MTSAT-1R SWIR at 02 UTC 7 Nov. 2007 (a) and fog detection results on IR1 image (b~f).

5. Problems and Area of Improvement

As fog has similar optical characteristics to the surface and cloud, it is very difficult to detect fog by satellite. In the case of fog that takes place locally, the detection is even harder due to the limitation of spatial resolution and navigation error. Therefore, in this algorithm, we acknowledged the limit of satellite detection, and focused on continuous detection of fog throughout the whole process such as formation, development and disappearance with a certain area and intensity. Low level cloud is another significant difficulty in fog detection using satellite image since it can be observed as fog in some occasions depending on the altitude of the area of observation. As cloud and fog has different optical properties depending on the particle size and optical thickness, fog properties on sea and land is different. In this algorithm, same algorithm and threshold were used for sea and land, containing more error of fog detection particularly in the sea. In the future, a detection algorithm is needed to be developed considering threshold calculation and properties of fog especially in the sea.

6. References

- Bendix, J., 2002; A satellite-based climatology of fog and low-level stratus in Germany and adjacent areas. *Atmos. Res.* 64. 3-18.
- Bendix, J., B. Thies, J. Cermak, and T. Naub, 2005: Ground Fog Detection from Space Based on MODIS Daytime Data-A Feasibility Study. *Wea. and Forecasting.* 20, 989-1005.
- Cermak, Jan, J. Bendix, 2008: A novel approach to fog/low stratus detection using Meteosat 8 data, *Atmos. Res.* 87, 279-292.
- Dybbroe, A., 1993. Automatic detection of fog at night using AVHRR data. *Proc. 6th AVHRR Data Users' Meeting*, pp. 245-252.
- Ellord, G. P., 1995: Advances in the detection and analysis of fog at night using GOES multispectral infrared imagery. *Wea. Forecasting*, 10, 606-619.
- Eyre, J. R., Brownscombe, J. L., Allam, R. J., 1984: Detection of fog at night using Advanced Very High Resolution Radiometer. *Meteorol. Mag.* 113, 266-271.
- Gultepe I., M. Pagowski, and J. Reid, 2007: A satellite-Based Fog Detection Scheme Using Screen Air Temperature.
- Lee, T. F., F. J. Turk, and K. Richardson, 1997: Stratus and fog products using GOES-8-9

- 3.9- μm data. *Wea. Forecasting*, 12, 664-677.
- Saunders, R. W., Kriebel, K. T., 1988: An improved method for detecting clear sky and cloudy radiances from AVHRR data. *Int. J. Remote Sens.* 9, 123-150.
- Schreiner A. J., S. A. Ackerman, B. A. Baum, and A. K. Heidinger, 2007: A Multispectral Technique for Detecting Low-Level Cloudiness near Sunrise, *J. Atmos. and Ocean. Tec.*, 24, 1800-1810.
- Turk, J., J. Vivekanandan, T. Lee, P. Durkee, and K. Nielsen, 1998: Derivation and Applications of Near-Infrared Cloud Reflectances from GOES-8 and GOES-9. *Amer. Meteor. Soc.*, 37, 819-831.
- Turner, J., Allam, R. J., Maine, D. R., 1986: A case study of the detection of fog at night using channel 3 and 4 on the Advanced Very High Resolution Radiometer (AVHRR). *Meteorol. Mag.* 115, 285-290.
- Wetzel, M. A., R. D. Vorys, and L. E. Xu, 1996: Satellite microphysical retrievals for land-based fog with validation by balloon profiling. *J. Appl. Meteor.*, 35, 810-829.